Tellus (1984), *36A*, 384–400

The effect of friction and topography on coastal internal Kelvin waves at low latitudes

By R. D. ROMEA[1] and J. S. ALLEN *School of Oceanography, Oregon State University, Corvallis, Oregon 97331, USA*

(Manuscript received June 7; in final form October 11, 1983)

ABSTRACT

The effects of bottom Ekman layer friction and slope topography on freely propagating coastal internal Kelvin waves in a stratified ocean are examined. Frictional effects are assumed weak and specific slope topographies are chosen so that perturbation methods may be used to obtain solutions. Two models for slope topography are utilized: a steep slope model, which corresponds to the low latitude case where the Rossby radius scale δ_R is assumed large compared to the slope width L_s, and a weak slope model, which corresponds to the case $\delta_R \ll L_s$. For both cases, internal Kelvin waves are damped by bottom friction, and offshore and vertical phase lags are induced, as well as an onshore flow. However, there are substantial differences between the results obtained with the two different models. For example, vertical phase shifts due to friction for the steep slope case imply that alongshore velocity v at the surface leads v below, while motions at the bottom lead for the weak slope case. For the weak slope, frictional effects are proportional to bottom velocity, implying that, for mid-latitudes, bottom stress effects on barocline modes are minimal. However, results from the steep slope model imply that baroclinic modes are significantly affected by bottom stress at low latitudes. In both cases, the topography changes the frequency and alongshore phase speed of the wave, the modal structure is altered, and an onshore flow is induced. For the weak slope case, the wave speed is proportional to the mean bottom depth averaged over the Rossby radius scale. For the steep slope, changes in wave speed depend on the details of the slope geometry: a slope that is concave downward increases the speed while a slope that is concave upward decreases the speed. Both models are compared with observations from the Peru coast.

1. Introduction

Evidence has been presented for the existence of coastally trapped waves along the central Peru coast (Smith, 1978), where observations indicate poleward propagation between 10° and 15° S of fluctuations in sea level, alongshore currents and temperature in the 0.1–0.2 cpd frequency band with phase speeds of about 200 km day^{-1}. Although the frequency range of the propagating fluctuations is similar to that of weather events, they are found to be uncorrelated with the local winds measured at 12° S or 15° 30′ S (Brink et al., 1978). The analysis has recently been extended equatorward and poleward by Romea and Smith (1983), and free waves are found to propagate poleward between 2° and 17° S.

In general, free coastally trapped waves have modal structures and phase speeds that are dependent on shelf topography, stratification, and latitude (see, e.g., Allen and Romea, 1980, for a detailed discussion of this point). The structure of the current fluctuations and the nature of the dynamical balances suggest that the waves observed along the Peru coast are internal Kelvin wave-like (Smith, 1978; Brink et al., 1978; Brink et al., 1980; Allen and Smith, 1981; Brink 1982a; Romea and Smith, 1983), i.e., that the density

[1] Present affiliation: Department of Oceanography Florida State University, Tallahassee, Florida 32306, USA.

stratification is the dominant mechanism for the waves, with the bottom topography inducing only a minor modification to their structure and dynamics. This observational result agrees with the conceptual model that the effect of the continental margin should be much like a vertical wall for low latitudes where the Rossby radius of deformation, δ_R, which is the natural baroclinic offshore length scale, is greater than the shelf-slope width L_s. Estimating the Rossby radius scale by $\delta_R = c/f$, where c is an alongshore phase speed and f the Coriolis parameter, we find, at 5° S latitude, with $f \simeq 1.3 \times 10^{-5}\ s^{-1}$ and $c \simeq 200$ km day^{-1}, that $\delta_R \simeq 180$ km, whereas $L_s \simeq 80$–100 km.

Phase shifts in the offshore and vertical directions have been observed in the velocity data from the Peru coast (Brink et al., 1978). For barotropic motions, Brink and Allen (1978) have shown that cross-shelf phase lags may be induced by the effect of bottom Ekman layer friction, and Brink et al. (1980) report an observed mean bottom Ekman layer thickness of 10–20 m based on the Peru data from March–May 1977. Thus, the observed phase shifts may be due to the effects of bottom friction.

Models with continuous stratification and realistic bottom topography are the most useful for direct comparison with coastally trapped wave observations at low latitudes. These models are generally intractable analytically and a numerical approach has been adopted in the past (e.g., Huthnance, 1978; Brink, 1982a). However, there are difficulties with numerical models for low latitudes where $L_s/\delta_R \ll 1$ (Brink, personal communication). In addition, if bottom friction effects are included, it is difficult to calculate numerically the structure of alongshore velocity accurately (Brink, 1982b).

Martinsen and Weber (1981) examined the influence of internal vertical friction on free internal Kelvin waves with a flat bottom. They separate in terms of vertical normal modes, which implies a stress-free bottom and which limits the formulation to a relatively deep ocean. For realistic continental shelf-slope regions, such a formulation may be inadequate, and hence we present a simple formulation for the study of the effects of botton friction coupled with shelf-slope topography on free Kelvin waves in a continuously stratified ocean.

We concentrate primarily on the low-latitude case with weak bottom friction effects and derive analytical results with a perturbation analysis for $L_s/\delta_R \ll 1$ and for $T_f/T \gg 1$, where T_f is the frictional time scale and T is the wave period. The limit $L_s/\delta_R \to 0$ corresponds to the flat bottom vertical wall case. As will be discussed, the formulation including the effect of bottom friction at low latitudes depends conceptually on taking the limit $T_f/T \to \infty$ before the limit $L_s/\delta_R \to 0$.

For comparison with the case $L_s/\delta_R \ll 1$, we also include results for $L_s/\delta_R \gg 1$, with a vertical wall and a weak slope. We also primarily consider $T_f/T \gg 1$. Phase lags induced by bottom friction are qualitatively different in this case and it is of interest to contrast these results with those from the low-latitude case.

2. Formulation

We consider a continuously stratified ocean on an f-plane in the northern hemisphere. Cartesian coordinates are utilized with x' positive westward, y' positive southward, and z' positive vertically upward. Primes denote dimensional quantities for which a non-dimensional counterpart will later be defined. The ocean is bounded on top by a rigid lid and on the bottom by a boundary at $z' = -H$. There is a straight north–south oriented eastern boundary at $x' = 0$. The problem is linearized by the assumption that the motion results in negligible non-linear fluid accelerations and in small departures ρ' from an equilibrium stable density distribution $\bar{\rho}(z')$. The hydrostatic approximation is utilized, and we consider interior motions away from frictional boundary layers. The long-wave assumptions for coastally trapped waves are made, i.e., the frequency ω of the wave motions is small compared to f, and the alongshore scale L_y of the waves is large compared to their offshore scale L.

Dimensionless variables are formed in the following manner:

$$(x,y) = (x',y')/L, \quad z = z'/H, \quad t = t'f,$$

$$(u,v) = (u',v')/U, \quad w = w'L/(HU), \tag{2.1}$$

$$p = p'/(\rho_0 UfL), \quad \rho = (\rho' gH)/(\rho_0 UfL).$$

The variables (u',v',w') are the velocity components in the (x',y',z') directions, t' is time, p' is the pressure, U is a characteristic horizontal velocity, and the total density is given by

$$\rho_T'(x',y',z',t') = \rho'(x',y',z',t') + \bar{\rho}(z') + \rho_0, \tag{2.2}$$

where ρ_0 is a constant.

With the above assumptions and scaling, the governing equations are

$$v = p_x, \tag{2.3a}$$

$$v_t + u = -p_y, \tag{2.3b}$$

$$0 = -p_z - \rho, \tag{2.3c}$$

$$\rho_t - R^2 w = 0, \tag{2.3d}$$

$$u_x + v_y + w_z = 0, \tag{2.3e}$$

where

$$R(z) = NH/(fL), \tag{2.4a}$$

$$N^2(z) = -g\bar{\rho}_z/\rho_0, \tag{2.4b}$$

and where the subscripts denote partial differentiation. $N^2(z)$ is the square of the Brunt–Väisälä frequency, and $R(z)$ is a stratification parameter that represents the ratio of the Rossby radius scale to L.

Eqs. (2.3a–e) may be combined into a single equation for the pressure given by

$$\{p_{xx} + [R^{-2}(z)p_z]_z\}_t = 0. \tag{2.5}$$

Boundary conditions for p, resulting from the assumption that the surface is a rigid lid, and a regularity condition that specifies coastal trapping, are respectively

$$p_{zt} = 0, \quad \text{at} \quad z = 0, \tag{2.6a}$$

$$p_x, p_y \to 0, \quad \text{as} \quad x \to \infty. \tag{2.6b}$$

The remaining boundary conditions depend on the specific bottom topography chosen, and will be introduced later.

3. Steep slope

The geometry of the steep slope model is shown in Fig. 1. The side wall, located at $x' = \varepsilon'(z)$, intersects the surface at $x' = 0, z' = 0$. We assume that the offshore scale of the slope topography is small compared to a characteristic offshore scale L, i.e., $\varepsilon = \varepsilon'/L \ll 1$, and that the slope intersects the bottom at $x = \varepsilon_0 \ll 1, z = -1$.

We introduce friction in the problem by assuming there are quasi-steady Ekman layers on the bottom at $z = -1$ and on the slope $x = \varepsilon(z)$. The boundary condition at $z = -1$, which represents the

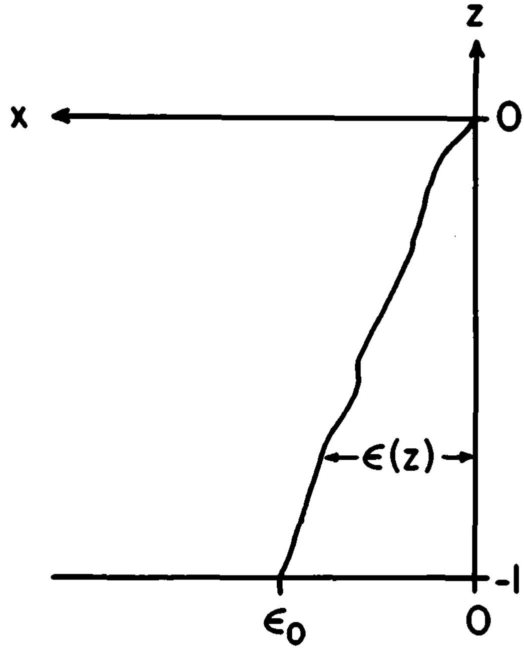

Fig. 1. Steep slope model.

Ekman compatibility condition (Pedlosky, 1979, Section 4.5) on the interior flow, is given by

$$p_{zt} = -\tfrac{1}{2}R^2 E_v^{1/2} p_{xx}, \quad \text{at} \quad z = -1, \tag{3.1a}$$

where

$$E_v^{1/2} = H^{-1}(2\,\nu_v/f)^{1/2}. \tag{3.1b}$$

E_v is the vertical Ekman number and ν_v is a constant vertical eddy coefficient.

A standard boundary layer analysis (e.g., Pedlosky, 1979, Section 4.9) for a constant sloping boundary, which will be valid for general slope topography as long as the radius of curvature is large compared to the boundary layer thickness, gives a normal layer thickness of $E_v^{1/2}(\cos\alpha')^{1/2}$, where α' is the dimensional slope angle. The normal velocity w_N at the top of the layer and the transport T_E parallel to the slope in the layer are given by

$$w_N = \tfrac{1}{2}E_v^{1/2} v_\zeta(\cos\alpha')^{-1/2}, \tag{3.2a}$$

$$T_E = -\tfrac{1}{2}E_v^{1/2} v(\cos\alpha')^{-1/2}, \tag{3.2b}$$

where ζ measures distance along the slope downward from the surface. The results (3.2a,b) are derived with the assumption that L is sufficiently large that $E_v/E_h = (\nu_v/\nu_h)(L/H)^2 \gg 1$, where ν_h is a constant horizontal eddy coefficient. This assumption has been discussed by Allen (1973) and Pedlosky (1974), and is equivalent to the statement that the offshore scale is large compared to the horizontal diffusion scale.

The alongshore velocity v at the top of the Ekman layer is given by

$$v = (\cos\alpha)^{-1} p_{\zeta} + (\tan\alpha) p. \tag{3.2c}$$

Note that we are considering a stratified interior and (3.2c) differs from the interior limit of (4.9.27b) in Pedlosky (1979) by virtue of (2.3c). Using (2.3c) in (3.2c) yields (2.3a) for v, as expected.

With the scaling given in (2.1) and with $\varepsilon \ll 1$, the magnitude of the slope angle α in the nondimensional system is such that

$$\tan\alpha = O(\varepsilon_0^{-1}) \gg 1. \tag{3.3a}$$

However, the problem is formulated such that $NH(f\pi)^{-1} \gg L \gg H$, i.e., that the shelf-slope width is much greater than the deep ocean depth but much less than the internal Rossby radius scale associated with the first baroclinic mode. Therefore

$$\tan\alpha' = O(H/L) \ll 1. \tag{3.3b}$$

In terms of variables in x and z,

$$w_N = u\sin\alpha + w\cos\alpha \tag{3.3c}$$

and

$$\partial/\partial\zeta = \cos\alpha(\partial/\partial x) - \sin\alpha\,(\partial/\partial z). \tag{3.3d}$$

Substituting (3.3c,d) in (3.2a), we obtain

$$u\sin\alpha + w\cos\alpha = \tfrac{1}{2}E_v^{1/2}(\cos\alpha')^{-1/2} \times (v_x\cos\alpha - v_z\sin\alpha), \quad \text{at} \quad x = \varepsilon(z). \tag{3.4a}$$

With (3.3a,c,d), (3.4a) is approximately

$$u = -\varepsilon_z w - \tfrac{1}{2}E_v^{1/2}(\cos\alpha')^{-1/2} v_z + O(\varepsilon_0) + O(E_v), \quad \text{at } x = \varepsilon(z). \tag{3.4b}$$

Typical values ($H \simeq 4$ km, $L \simeq 100$ km) give $\alpha' \simeq 2.3°$, so that the dimensional slope appears locally almost horizontal. Thus, we anticipate that the bottom Ekman layer will extend over the slope up to the surface. With $\cos\alpha' \simeq 1$ and at $x = \varepsilon(-1)$, the Ekman layer transport (3.2b) on the slope is approximately equal to the Ekman layer transport on the flat bottom. Since the fluxes approximately match where the slope meets the bottom, there will be negligible flux into the interior due directly to the change in slope, although there will be a discontinuity in normal velocity. With no wind stress forcing, and hence no flux in the surface Ekman layer, any net flux into the Ekman layer along the flat bottom or along the slope must be pumped out at $x = 0$, $z = 0$. The approximate boundary condition for p along the sloping boundary, from (3.4b) is thus

$$p_{xt} + p_y = \varepsilon_z R^{-2} p_{zt} + \tfrac{1}{2}E_v^{1/2}[p_{xz} - p_{x(0)}\delta(z)], \quad \text{at} \quad x = \varepsilon(z), \tag{3.4c}$$

where $p_{x(0)} = p_x(x = 0,\ z = 0)$. This condition specifies that the onshore flow in the interior is balanced by the inviscid vertical velocity produced by the slope plus the Ekman pumping along the slope. The last term on the right-hand side of (3.4c) represents the flow out of the Ekman layer at $x = 0$, $z = 0$ and *must* be included so that the mass flux condition

$$\int_\Gamma w_N \mathrm{d}\hat{s} = 0 \tag{3.4d}$$

is satisfied, where Γ is the lower boundary, and $\hat{s}$ is distance along the boundary (see comment after eq. (3.27)). The function δ is defined here such that $\delta(z) = 0$ for $z \neq 0$ and

$$\int_{-1}^{0} \delta(z)\mathrm{d}z = 1. \tag{3.4e}$$

We seek a free wave solution of the form

$$p(x,y,z,t) = \mathrm{Re}\,\{\phi(x,z)\exp[-i(\omega t + ly)]\}, \tag{3.5}$$

where ω and l are radian frequency and alongshore wave number, respectively. Substituting (3.5) in (2.5), (2.6a,b), (3.1a) and (3.4b), we obtain

$$\phi_{xx} + (\phi_z/R^2)_z = 0, \tag{3.6}$$

$$\phi_z = 0, \quad \text{at} \quad z = 0, \tag{3.7a}$$

$$\phi_z = -\tfrac{1}{2}i\lambda R^2\phi_{xx}, \quad \text{at} \quad z = -1, \tag{3.7b}$$

$$\phi_x + (l/\omega)\phi = \varepsilon_z R^{-2}\phi_z + \tfrac{1}{2}i\lambda[\phi_{xz} - \phi_{x(0)}\delta(z)], \quad \text{at} \quad x = \varepsilon(z), \tag{3.7c}$$

$$\phi_x \to 0, \quad \text{as} \quad x \to \infty, \tag{3.7d}$$

where, as in (3.4b), the notation $\phi_{x(0)}$ implies $\phi_x(x = 0,\ z = 0)$, and where $\lambda = E_v^{1/2}/\omega$. Eqs. (3.6) and (3.7a–d) describe an eigenvalue problem for ϕ with complex eigenvalue ω.

To proceed, we first transform the boundary conditions at $x = \varepsilon(z)$ to hold on a constant surface

$\xi = 0$ by defining a new coordinate system (ξ, y, z), where

$$\xi = x - \varepsilon(z). \tag{3.8}$$

A similar transformation has been used by Huthnance (1978) to handle boundary conditions similar to (3.7c). The surfaces $z = 0, -1$ remain unaffected by the coordinate transformation.

The transformed equations and boundary conditions are

$$\phi_{\xi\xi} + (\phi_z/R^2)_z + (\varepsilon_z/R)^2\phi_{\xi\xi} - 2\varepsilon_z R^{-2}\phi_{\xi z} - (\varepsilon_z/R^2)_z\phi_\xi = 0, \tag{3.9}$$

$$\phi_z - \varepsilon_z\phi_\xi = 0, \quad \text{at} \quad z = 0, \tag{3.10a}$$

$$\phi_z - \varepsilon_z\phi_\xi = -\tfrac{1}{2}i\lambda R^2\phi_{\xi\xi}, \quad \text{at} \quad z = -1, \tag{3.10b}$$

$$\phi_\xi + (l/\omega)\phi = \varepsilon_z R^{-2}(\phi_z - \varepsilon_z\phi_\xi) + \tfrac{1}{2}i\lambda\{\phi_{\xi z} - \varepsilon_z\phi_{\xi\xi} - \phi_{\xi(0)}\delta(z)\}, \quad \text{at} \quad \xi = 0, \tag{3.10c}$$

$$\phi_\xi \to 0, \quad \text{as} \quad \xi \to \infty. \tag{3.10d}$$

A relatively simple solution to (3.9) and (3.10) may be obtained by perturbation methods. We assume $\lambda = O(\varepsilon_o) \ll 1$, which corresponds to limiting the wave period to be much less than the spin down time. In addition, it is important that the limits $\lambda \to 0$, $\varepsilon \to 0$ be taken in that order, since if $\varepsilon \to 0$, $\lambda \neq 0$, the Ekman layer on the slope would vanish and (3.10c) would be incorrect.

The variables are expanded as

$$\phi = \phi^{(0)} + \phi^{(1)} + \ldots, \tag{3.11a}$$

$$\omega = \omega^{(0)} + \omega^{(1)} + \ldots, \tag{3.11b}$$

where $\phi^{(0)}$ and $\omega^{(0)}$ are assumed to be O(1) and $\phi^{(1)}$ and $\omega^{(1)}$ are assumed to be $O(\varepsilon_0)$. If (3.11a, b) are substituted in (3.9) and (3.10), the lowest-order balance is the familiar inviscid internal Kelvin wave problem, i.e.,

$$\phi^{(0)}_{\xi\xi} + (\phi^{(0)}_z/R^2)_z = 0, \tag{3.12}$$

$$\phi^{(0)}_z = 0, \quad \text{at} \quad z = 0, -1, \tag{3.13a}$$

$$\phi^{(0)}_\xi + (l/\omega^{(0)})\phi^{(0)} = 0, \quad \text{at} \quad \xi = 0, \tag{3.13b}$$

$$\phi^{(0)}_\xi \to 0, \quad \text{as} \quad \xi \to \infty, \tag{3.13c}$$

with solutions

$$\phi^{(0)}_n = \exp(-l\xi/\omega^{(0)}_n)P_n(z), \tag{3.14}$$

where

$$(P_{nz}/R^2)_z + (l/\omega^{(0)}_n)^2 P_n = 0, \tag{3.15}$$

$$P_{nz} = 0, \quad \text{at} \quad z = 0, -1. \tag{3.16}$$

Eqs. (3.15) and (3.16) form an eigenvalue problem with eigenfunctions P_n and real eigenvalues $\omega^{(0)}_n$. The eigenfunctions form a complete set and are orthogonal over the domain $(-1, 0)$ subject to

$$\int_{-1}^{0} P_n P_m \, dz = \delta_{nm}, \tag{3.17}$$

where δ_{nm} is the Kronecker delta. An additional restriction due to (3.13c) is $l/\omega^{(0)}_n > 0$, which implies that the waves travel only poleward. These results have been obtained for general subinertial coastally trapped waves (see, e.g., Huthnance, 1975, and Clarke, 1977).

The equations describing the $O(\varepsilon_0)$ correction to each mode n, where terms of $O(\varepsilon_0^2)$, $O(\lambda^2)$, and $O(\lambda\varepsilon)$ have been neglected, are

$$\phi^{(1)}_{n\xi\xi} + (\phi^{(1)}_{nz}/R^2)_z = 2\varepsilon_z R^{-2}\phi^{(0)}_{n\xi z} + (\varepsilon_z/R^2)_z\phi^{(0)}_{n\xi}, \tag{3.18}$$

$$\phi^{(1)}_{nz} = \varepsilon_z\phi^{(0)}_{n\xi}, \quad \text{at} \quad z = 0, \tag{3.19a}$$

$$\phi^{(1)}_{nz} = \varepsilon_z\phi^{(0)}_{n\xi} - \tfrac{1}{2}i\lambda^{(0)}_n R^2\phi^{(0)}_{n\xi\xi}, \quad \text{at} \quad z = -1, \tag{3.19b}$$

$$\phi^{(1)}_{n\xi} + (l/\omega^{(0)}_n)\phi^{(1)}_n = l(\omega^{(1)}_n/\omega^{(0)2}_n)\phi^{(0)}_n + \varepsilon_z R^{-2}\phi^{(0)}_{nz} + \tfrac{1}{2}i\lambda^{(0)}_n\{\phi^{(0)}_{n\xi z} - \phi^{(0)}_{n\xi(0)}\delta(z)\}, \quad \text{at} \quad \xi = 0, \tag{3.19c}$$

$$\phi^{(1)}_{n\xi} \to 0, \quad \text{as} \quad \xi \to \infty, \tag{3.19d}$$

where

$$\lambda^{(0)}_n = E_v^{\frac{1}{2}}/\omega^{(0)}_n. \tag{3.19e}$$

A compatibility condition for the solution $\phi^{(1)}_n$ may be found by multiplying (3.18) by $\phi^{(0)}_n$, integrating over ξ from 0 to ∞ and over z from -1 to 0, and utilizing the boundary conditions (3.13a, b, c), and (3.19a–d). This determines $\omega^{(1)}_n$ as

$$\omega^{(1)}_n = -\tfrac{1}{4}i\lambda^{(0)}_n[P^2_{n(0)} + P^2_{n(-1)} + R^2_{(-1)}(\omega^{(0)}_n/l)^2 I_{nn}] \times \omega^{(0)}_n - (\omega^{(0)2}_n/l)\int_{-1}^{0} \varepsilon_z R^{-2} P_{nz} P_n dz, \tag{3.20}$$

where

$$I_{nm} = \int_{-1}^{0} \{(P_{nz}/R^4)_z - (l/\omega^{(0)}_n)^2(z/R^2)_z P_n\} P_m dz, \tag{3.21}$$

and where the P_n are determined by (3.15), (3.16) and (3.17). The solution to (3.18) and (3.19) is

$$\phi^{(1)}_n = \varepsilon\phi^{(0)}_{n\xi} - \tfrac{1}{2}i\lambda^{(0)}_n(R^2_{(-1)}/R^2)z\phi^{(0)}_{nz} + \psi_n, \tag{3.22}$$

$$\psi_n = \sum_{m=0}^{\infty} \gamma_m(\xi) P_m(z), \tag{3.23a}$$

where, $P_0 = 1$ and

$$\gamma_m = A_m \exp(-l\xi/\omega_m^{(0)}) + B_m \exp(-l\xi/\omega_n^{(0)}), \tag{3.23b}$$

$$A_m = [(l/\omega_n^{(0)}) - (l/\omega_m^{(0)})]^{-1} \times \{\int_{-1}^{0} \varepsilon_z R^{-2} P_{nz} P_m \,dz - \tfrac{1}{2} i\lambda_n^{(0)} (l/\omega_n^{(0)}) \times (\int_{-1}^{0} P_{nz} P_m \,dz - P_{n(0)} P_{m(0)})\}, \quad m \neq n, m \geqslant 1, \tag{3.23c}$$

$$B_m = \tfrac{1}{2} i\lambda_n^{(0)} R_{(-1)}^2 [(l/\omega_n^{(0)})^2 - (l/\omega_m^{(0)})^2]^{-1} I_{nm}, \tag{3.23d}$$

$$\gamma_0 = (\omega_n^{(0)}/l) \int_{-1}^{0} \varepsilon_z R^{-2} P_{nz} \,dz + \tfrac{1}{2} i\lambda_n^{(0)} [P_{n(-1)} + (\omega_n^{(0)}/l)^2 R_{(-1)}^2 I_{n0} \exp(-l\xi/\omega_n^{(0)})], \tag{3.23e}$$

$$\gamma_n = -\tfrac{1}{4} i\lambda_n^{(0)} (\omega_n^{(0)}/l) R_{(-1)}^2 \xi \exp(-l\xi/\omega_n^{(0)}) I_{nn}. \tag{3.23f}$$

The coefficient of the homogeneous solution to (3.18) and (3.19) is abritrary and the homogeneous solution may be absorbed in the O(1) solution. The $m = 0$ term in (3.23) represents a barotropic flow induced by friction and topography.

Since the $\omega_n^{(0)}$ are ordered such that $\omega_n^{(0)} \to 0$ as $n \to \infty$, the perturbation procedure becomes invalid for high mode number, i.e., when $\lambda_n^{(0)} = E_v^{1/2}/\omega_n^{(0)} = O(1)$ and when $\delta_R/\varepsilon_0 = \omega_n^{(0)}(l\varepsilon_0)^{-1} = O(1)$. Therefore we must restrict our consideration to low modes where $\lambda^{(0)} \ll 1$ and $\delta_R/\varepsilon_0 \gg 1$. This restriction is not too severe, since we are generally only interested in the behaviour of the first mode.

The frictional correction to the O(1) eigenfunction is $O(\lambda_n^{(0)})$ and is purely imaginary, while the topographic correction is $O(\varepsilon_0)$ and is real. To $O(\lambda_n^{(0)})$, $O(\varepsilon_0)$, the presence of bottom friction induces phase shifts in x and z but does not change the x, z structure of v or p, while the slope topography affects the x, z structure of v and p but not the phase. Both friction and topography induce corrections to the frequency. The $O(\lambda_n^{(0)})$ frictional correction (from the first three terms on the right-hand side of (3.20)) is purely imaginary and represents a frictional decay or "spin-down" with time. The last term on the right-hand side of (3.20) represents a correction to the real free wave speed due to the slope topography. The contribution of that term may be seen by multiplying (3.15) by P_{nz}/R^2 and integrating over z from -1 to 0, to obtain, after integration by parts and the use of (3.16),

$$\int_{-1}^{0} R^{-2} P_{nz} P_n \,dz = 0. \tag{3.24}$$

Eq. (3.24) is a statement that the vertical velocity ($\simeq R^{-2} P_{nz}$) and the topographically-induced onshore velocity ($\simeq P_n$) are orthogonal over the depth. This implies together with the last term in (3.20) that, for a linear slope, i.e., for

$$\varepsilon(z) = -\varepsilon_0 z, \tag{3.25}$$

where $\varepsilon_z = -\varepsilon_0 =$ constant, the interaction between u and w averaged over the slope is zero, so that the topographic correction to the phase speed is zero. There is still a distortion of the mode shape, however. For a slope with curvature, corrections to both modal structure and phase speed are induced.

For an arbitrary stratification, the eigenfunctions P_n and eigenvalues may be computed numerically from (3.15), (3.16), and (3.17). A simple case, for which eigenfunctions and eigenvalues may be obtained directly, is $R = R_0 =$ constant, which corresponds to a constant Brunt–Väisälä frequency. While this case is generally unrealistic (the modal amplitude for $z < -\tfrac{1}{2}$ tends to be overestimated), it is useful for obtaining solutions that illustrate the essential physics. Solutions with a more realistic stratification are obtained in the Appendix and are discussed in Section 5.

With $R = R_0$, (3.14)–(3.17) give

$$\phi_n^{(0)} = 2 \exp(-n\pi\xi/R) \cos(n\pi z), \tag{3.26a}$$

$$\omega_n^{(0)} = lR/(n\pi), \quad n = 1, 2, 3, \ldots, \tag{3.26b}$$

and the correction to the frequency from (3.20) is

$$\omega_n^{(1)} = -\tfrac{1}{2} i E_v^{\frac{1}{2}} + 2(\omega_n^{(0)}/R) \int_{-1}^{0} \varepsilon_z \sin n\pi z \cos n\pi z \,dz. \tag{3.27}$$

Using (3.26a, b), the next order correction (3.22) may be calculated directly. Substitution of (3.27) in (3.5) shows that the $O(\lambda_n^{(0)})$ correction to the frequency represents a frictional decay with time, where the wave damping is given by $\exp(-\tfrac{1}{2} E_v^{\frac{1}{2}} t)$. Note that, if the first term in (3.20), which comes from the δ function in (3.4c), were not included, the frictional correction to ω would imply an exponential *growth* instead of decay.

We next examine the effect of bottom friction on the first vertical mode for the special case $R = R_0$ and $\varepsilon(z)$ given by (3.25) (a linear slope topography). The $n = 1$ eigenfunction may be written, to $O(\varepsilon_0)$ and $O(\lambda_n^{(0)})$, as

$$\phi_1 = |\phi_1| \exp(i\theta_1), \tag{3.28}$$

where

$$|\phi_1| = |\phi_1^{(0)}(1 + \varepsilon_0 \pi z/R) - 2\varepsilon_0(\pi R)^{-1}(1 + 2S)|, \tag{3.29a}$$

$$\theta_1 = \tan^{-1}\{\tfrac{1}{2}\lambda_1^{(0)}[-1 + \exp(-\pi\xi/R) \times (\pi z \sin \pi z + (\pi\xi/R)\cos \pi z) + 4S + D]/\phi_1^{(0)}\}, \tag{3.29b}$$

$$S = -\sum_{k=1}^{\infty} \phi_{2k}^{(0)}(1 - 2k)^{-1}(1 - 4k^2)^{-1}, \tag{3.29c}$$

$$D = 2\sum_{k=2}^{\infty} (1 - k)^{-1}\phi_k^{(0)}. \tag{3.29d}$$

The polar representation for ϕ_1 ((3.28) and (3.29)) shows that there is an $O(\lambda_1^{(0)})$ phase shift in both the x and z directions. The dependence on λ indicates that the effect of friction is enhanced for higher latitude or lower frequency. Note that, if x and ε_0 are rescaled with R/π ($x^* = \pi x/R$, $\varepsilon_0^* = \pi\varepsilon_0/R$, $\xi^* = \pi\xi/R$), $\lambda_1^{(0)}$ and ε^* are the only parameters in (3.29).

The x, z structure of the correction to the alongshore velocity, computed using (2.3a) and (3.28), is given by

$$\phi_{1x} = (|\phi_1|_x + i|\phi_1|\theta_{1x}) \exp(i\theta_1). \tag{3.30}$$

The simple relationship between pressure and alongshore velocity for an inviscid internal Kelvin wave, i.e., $\phi_x = -(\pi/R)\phi$, is modified by the introduction of topographic and frictional effects. This behaviour has been noted by Brink (1982b).

Fig. 2 shows the frictionally-induced phase shift in p and v for the first mode internal Kelvin wave in the x^*–z plane for $\lambda_1^{(0)} = 0.1$, topography given by (3.25) with $\varepsilon^* = \pi\varepsilon_0/R = 0.1$, and $R = R_0$. With (3.28) and (3.5), $\theta_1 > \theta_2$ implies 1 lags 2. Phase shifts for v and p are clearly different; however, vertical phase shifts imply that both surface v and p lead those below. The 180° phase shift in the vertical is due to the structure of the first mode inviscid internal Kelvin wave, which has a zero crossing at $z = -\tfrac{1}{2}$, and would have an abrupt 180° phase shift at $z = -\tfrac{1}{2}$.

The offshore phase structure for both p and v is depth dependent. In the upper half (near surface), p offshore lags p at the coast, while the effect is reversed for the lower layer. For v, inshore motions lead for $-0{\cdot}15 < z < 0$ (near the surface), while offshore motions lead those near-shore for $-0{\cdot}15 > z > -0.5$. Phase shifts with x^* are small for $z < -0.5$, with a suggestion that near-shore motions lead except very near the bottom.

We next consider the effect of slope topography alone on the first mode internal Kelvin wave. Fig. 3 shows that x^*–z structure of v for the $n = 1$ mode

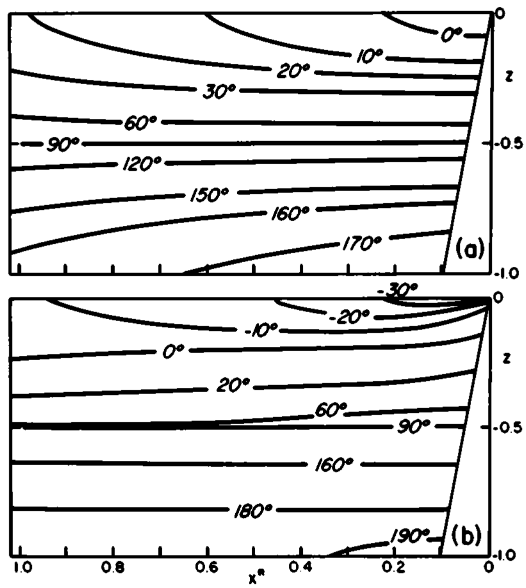

Fig. 2. Frictionally-induced phase shift θ (in degrees) in (a) p and (b) v for the $n = 1$ internal Kelvin wave in the x^*–z plane for $\lambda_1^{(0)} = 0.1$, topography (3.25) with $\varepsilon_0^* = 0.1$, and $R = R_0$ = constant. $\theta_1 > \theta_2$ implies 1 lags 2. Steep slope model.

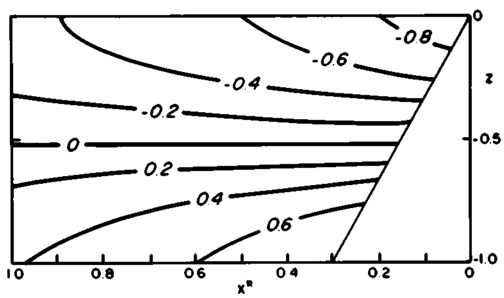

Fig. 3. x^*–z amplitude structure of v for the $n = 1$ internal Kelvin wave for $\lambda_1^{(0)} = 0$, topography (3.25) with $\varepsilon_0^* = 0.3$, and $R = R_0$. Steep slope model.

for $\lambda = 0$, (3.25) with $\varepsilon_0^* = 0.3$, and $R = R_0$. The alongshore velocity is not symmetric about the line $z = -\frac{1}{2}$, as would be expected with a vertical wall. Fig. 4 shows several examples of shelf shope topographies and Table 1 lists the $O(\varepsilon_0)$ topographic corrections to the $O(1)$ phase speed $c_n^{(0)}$ for each profile in Fig. 4. For each case, the shelf-slope width at $z = -1$ is ε_0^*, and $R = R_0$. The second term on the right-hand side of (3.27), which represents the topographic correction to ω for $R = R_0$, yields the result that slope profiles that are concave downward (case (a), Fig. 4) act to increase the free wave phase speed while profiles that are concave upward (case (b)) act to decrease the phase speed. As expected, the special case ε_z = constant (case (c)) gives no correction to the phase speed at $O(\varepsilon_0)$. Most shelf-slope topographies in nature are concave downward.

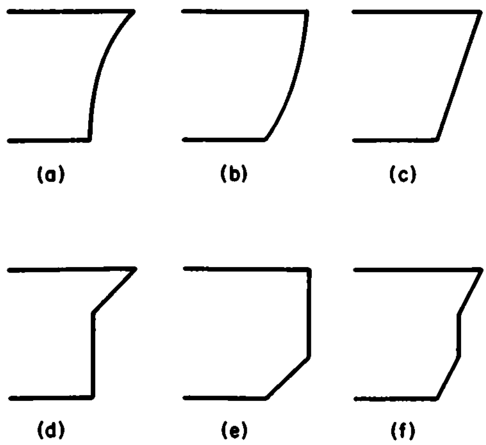

Fig. 4. Various slope topographies. The letters correspond to the cases discussed in Section 3 and listed in Table 1; (a) slope profile that is concave downward, (b) slope profile that is concave upward, (c) linear slope.

The change of sign of the correction to $c_n^{(0)}$ for cases (d) and (e) may be explained in the following manner. For an internal Kelvin wave over a flat bottom with a vertical wall and with constant N, the phase speed is given by $c_n = NH(n\pi)^{-1}$. With a small shallow shelf which drops steeply to a deep ocean (case (d)), the wave "rides" on the bottom at $x > \varepsilon_0$ and the shelf acts as an additional fluid volume which augments the effective depth by an $O(\varepsilon_0)$ amount, thus increasing the phase speed. For case (e), the small topography near the bottom decreases the effective depth by an $O(\varepsilon_0)$ amount, thus decreasing the phase speed. Cases (d) and (e) may be regarded as limiting cases of (a) and (b), respectively.

For case (f), two linear slopes interrupted by a segment of vertical wall, the wave identifies the vertical segment as a coastal boundary; the additional fluid volume provided by the shelf for $0 > z > -|z_0|$ is cancelled by the decrease due to the shelf segment for $-|z_0| > z > -1$, and the phase speed is unaffected to $O(\varepsilon_0)$. For case (c), the linear slope, there is no equivalent vertical wall to provide a reference zero for the mode. Case (c) may be viewed as a limit of case (f) as the vertical segment shrinks to zero. The addition of fluid volume for $0 > z > -\frac{1}{2}$ is exactly cancelled by the decrease of fluid volume for $-\frac{1}{2} > z > -1$. The effective depth and hence the phase speed remain unchanged.

Table 1. *$O(\varepsilon_0)$ topographic corrections $c_n^{(1)}$ to the $O(1)$ phase speeds $c_n^{(0)}$ for each of the profiles $\varepsilon(z)$ shown in Fig. 4; for each case, $\lambda = 0$, the shelf-slope width at $z = -1$ is ε_0, and $R = R_0$.*

Case	$\varepsilon(z)$	$c_n^{(1)}$
(a)	$-2\varepsilon_0(z + \frac{1}{2}z^2)$	$c_n^{(0)}\varepsilon_0(n\pi R)^{-1}$
(b)	$\varepsilon_0 z^2$	$-c_n^{(0)}\varepsilon_0(n\pi R)^{-1}$
(c)	$-\varepsilon_0 z$	0
(d)	$-\varepsilon z/\lvert z_0\rvert;\quad 0 \geqslant z > -\lvert z_0\rvert$ $\varepsilon_0;\quad -\lvert z_0\rvert > z \geqslant -1$	$c_n^{(0)}\varepsilon_0[1 - \cos(2n\pi\lvert z_0\rvert)](2n\pi R\lvert z_0\rvert)^{-1}$
(e)	$\varepsilon_0;\quad 0 \geqslant z > (-1 + \lvert z_0\rvert)$ $-\varepsilon_0(z + 1 - \lvert z_0\rvert)/\lvert z_0\rvert;\quad (-1 + \lvert z_0\rvert) > z \geqslant -1$	$-c_n^{(0)}\varepsilon_0[1 - \cos(2n\pi\lvert z_0\rvert)](2n\pi R\lvert z_0\rvert)^{-1}$
(f)	$-\varepsilon_0 z/\lvert z_0\rvert;\quad 0 \geqslant z > -\lvert z_0\rvert$ $\varepsilon_0;\quad -\lvert z_0\rvert > z > (-1 + \lvert z_0\rvert)$ $-\varepsilon_0(z + 1 - \lvert z_0\rvert)/\lvert z_0\rvert;\quad (-1 + \lvert z_0\rvert) > z \geqslant -1$	0

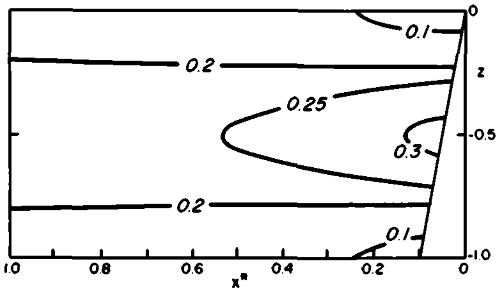

Fig. 5. Topographically-induced scaled onshore first mode velocity u/ε_0 in the x^*–z plane for $\lambda = 0$, topography (3.25) with $\varepsilon_0^* = 0.1$, and $R = R_0$. Steep slope model.

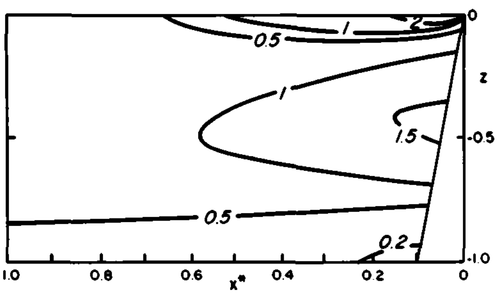

Fig. 6. First mode u/ε^* in the x^*–z plane for $\lambda_1^{(0)} = \varepsilon_0 = 0.1$, topography (3.25), and $R = R_0$. Steep slope model.

The onshore flow u may be obtained by solving (2.3a, b) with (3.5) for u in terms of ϕ. While there is no onshore flow associated with an internal Kelvin wave over a flat bottom, the presence of a steep slope induces a u of $O(\varepsilon_0)$ while friction induces a u of $O(\lambda_n^{(0)})$. Fig. 5 shows u/ε_0^* in the x^*–z plane with $\lambda_n^{(0)} = 0$, (3.25) with $\varepsilon_0^* = 0.1$, and $R = R_0$, i.e., this is the onshore flow induced by the topography alone. There is a maximum at $x^* = \varepsilon_0^*$, near $z = -\frac{1}{2}$, reflecting the interaction of the slope topography with the O(1) w which has a maximum near $z = -\frac{1}{2}$. Fig. 6 shows the amplitude of u/ε_0^* in the x^*–z plane where we have chosen $\lambda_n^{(0)} = \varepsilon_0^* = 0.1$, and $R = R_0$, so that both topography and friction are important. A local maximum of u near $z = -\frac{1}{2}$, $x^* = \varepsilon_0^*$ is again evident, and is enhanced relative to u in Fig. 5 due to the Ekman pumping along the sloping boundary. The relatively large u near $x^* = 0$, $z = 0$ is due to the mass flux out of the Ekman layer at that location required to satisfy (3.4).

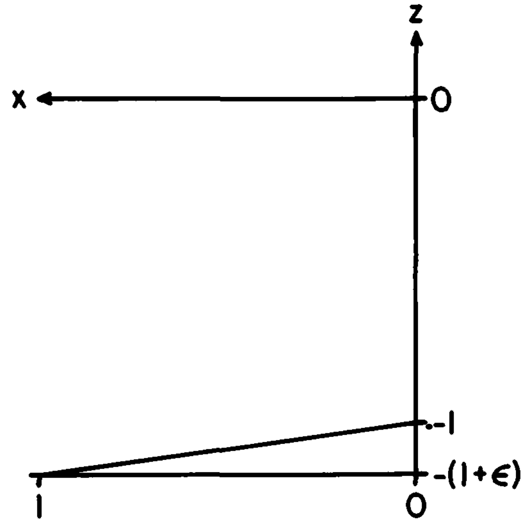

Fig. 7. Weak slope model.

4. Weak slope

The weak slope model shown in Fig. 7 represents the case where the Rossby radius scale is much smaller than the shelf-slope width, appropriate for mid-latitudes or for very wide shelves. In the model, the continental shelf-slope region is represented by a linear bottom slope of small magnitude, i.e., by

$$H(x) = 1 + \varepsilon x, \tag{4.1}$$

where ε is a constant and $\varepsilon \ll 1$. While the vertical wall at $x = 0$ is unrealistic, such geometries are commonly utilized for mid-latitude models; it is therefore of interest to compare their results with the steep slope model of Section 3.

The analysis proceeds as in Section 3, with weak friction, i.e., where $\lambda = O(\varepsilon)$, except that here the limits $\varepsilon \to 0$, $\lambda \to 0$ may be taken independently. The governing equation (2.5) and the boundary conditions (2.6a, b) apply. The boundary condition on the lower boundary, which represents the Ekman compatibility on the interior flow plus the invisicid boundary condition appropriate for a sloping boundary, is

$$p_{zt} + R^2 H_x (p_{xt} + p_y) = -\tfrac{1}{2} R^2 E_v^{1/2} p_{xx}, \quad \text{at} \quad z = -H(x). \tag{4.2}$$

The boundary condition that holds at $x = 0$ is

$$p_{xt} + p_y = -\tfrac{1}{2}E_v^{1/2} p_x(z=-1)\,\delta(z+1), \quad \text{at } x = 0, \tag{4.3a}$$

where $\delta(z+1)$ is equal to 0 for $z \neq -1$, and

$$\int_{-1}^{0} \delta(z+1)\,dz = 1. \tag{4.3b}$$

The term on the right-hand side of (4.3a) is due to the flow out of the Ekman layer at $x = 0$ and must be included so that the mass flux condition

$$\int_{-1}^{0} w(z=-1)\,dx + u(z=-1) = 0 \tag{4.4}$$

is satisfied. This is analogous to (3.4c) for the steep slope case, and, as in Section 3, neglect of this term leads to an exponential growth of the solution with time.

We seek a free wave solution given by (3.5). Substituting (3.5) in (2.5), (2.6a, b), (4.2) and (4.3a), we obtain (3.6), (3.7a), (3.7d) plus

$$\phi_x + (l/\omega)\phi = -\tfrac{1}{2}i\lambda\phi_x(z=-1)\,\delta(z+1), \quad \text{at} \quad x = 0, \tag{4.5a}$$

$$\phi_z = -R^2 H_x[\phi_x + (l/\omega)\phi] - \tfrac{1}{2}iR^2\lambda\phi_{xx}, \quad \text{at} \quad z = -H(x). \tag{4.5b}$$

We define the new coordinate system (x, y, η), where

$$\eta = z/H(x), \tag{4.6}$$

so that the lower boundary $z = -H(x)$ becomes $\eta = -1$ while the upper surface $z = 0$ becomes $\eta = 0$, i.e., the upper surface is unchanged. Transforming the equations and boundary conditions, we have

$$\begin{aligned}&\phi_{xx} + 2\eta\varepsilon^2(1 - 2\varepsilon x + \dots)\phi_\eta \\ &\quad - 2\eta\varepsilon(1 - \varepsilon x + \dots)\phi_{\eta x} \\ &\quad + (\eta\varepsilon)^2(1 - 2\varepsilon x + \dots)\phi_{\eta\eta} + (\phi_\eta/R^2)_\eta \\ &\quad \times (1 - 2\varepsilon x + \dots) = 0,\end{aligned} \tag{4.7}$$

$$\phi_\eta = 0, \quad \text{at} \quad \eta = 0, \tag{4.8a}$$

$$\begin{aligned}&\phi_x - \eta\varepsilon(1 - \varepsilon x + \dots)\phi_\eta + (l/\omega)\phi = -\tfrac{1}{2}i\lambda[\phi_x \\ &\quad + \eta\varepsilon(1 - \varepsilon x + \dots)\phi_{\eta(-1)}\,\delta(\eta+1)], \quad \text{at} \quad x = 0,\end{aligned} \tag{4.8b}$$

$$\begin{aligned}\phi_\eta &= -R^2\varepsilon(1 + \varepsilon x) \\ &\quad \times [\phi_x + (l/\omega)\phi - \eta\varepsilon(1 - \varepsilon x + \dots)\phi_\eta] \\ &\quad - \tfrac{1}{2}i\lambda R^2[\phi_{xx} + 2\eta\varepsilon^2(1 - 2\varepsilon x + \dots)\phi_\eta \\ &\quad - 2\eta\varepsilon(1 - \varepsilon x + \dots)\phi_{\eta\xi} + (\eta\varepsilon)^2(1 - 2\varepsilon x + \dots) \\ &\quad \times \phi_{\eta\eta}], \quad \text{at} \quad \eta = -1,\end{aligned} \tag{4.8c}$$

plus (3.7d) which is the coastal trapping condition. In (4.8b), $\phi_{\eta(-1)} = \phi_\eta(\eta = -1)$.

We expand ϕ and ω as in (3.11a, b), with the restrictions $\lambda \ll 1$, $x \leqslant O(1)$. The lowest order equations for $\phi^{(0)}$ give (for $n \geqslant 1$) the inviscid internal Kelvin wave problem (3.12), (3.13a, b, c) with a sequence n of solutions given by (3.14), (3.15) and (3.16) (with z replaced by η), orthogonal, subject to (3.17). The $n = 0$ solution is barotropic motion that corresponds to self waves (Allen, 1975; Allen and Romea, 1980). This barotropic mode is not studied here.

The $O(\varepsilon)$, $O(\lambda)$ balance, neglecting $O(\varepsilon^2)$, $O(\lambda^2)$, and $O(\varepsilon\lambda)$ is

$$\phi^{(1)}_{nxx} + (\phi^{(1)}_{n\eta}/R^2)_\eta = 2\varepsilon[\eta\phi^{(0)}_{nx\eta} + x(\phi^{(0)}_{n\eta}/R^2)_\eta], \tag{4.9}$$

$$\phi^{(1)}_{n\eta} = 0, \quad \text{at} \quad \eta = 0, \tag{4.10a}$$

$$\begin{aligned}&\phi^{(1)}_{nx} + (l/\omega^{(0)}_n)\phi^{(1)}_n = \eta\varepsilon\phi^{(0)}_{n\eta} + l(\omega^{(1)}_n/\omega^{(0)2}_n)\phi^{(0)}_n \\ &\quad - \tfrac{1}{2}i\lambda^{(0)}_n\phi^{(0)}_{nx(-1)}\,\delta(\eta+1), \quad \text{at} \quad x = 0,\end{aligned} \tag{4.10b}$$

$$\phi^{(1)}_{n\eta} = -\tfrac{1}{2}iR^2\lambda^{(0)}_n\phi^{(0)}_{nxx}, \quad \text{at} \quad \eta = -1, \tag{4.10c}$$

$$\phi^{(1)}_{nx} \to 0, \quad \text{as} \quad x \to \infty. \tag{4.10d}$$

The frequency correction is specified by the compatibility condition as in Section 3, and is

$$\begin{aligned}\omega^{(1)}_n &= (\omega^{(0)2}_n/l)\{\tfrac{1}{2}\varepsilon - \tfrac{1}{2}i\lambda^{(0)}_n \\ &\quad \times [\tfrac{1}{2}(\omega^{(0)}_n/l)R^2_{(-1)}I_{nn} + (l/\omega^{(0)}_n)P^2_{n(-1)}]\},\end{aligned} \tag{4.11}$$

where I_{nn} is given by (3.21) with z replaced by η.

The solution to (4.9) and (4.10) is

$$\phi^{(1)}_n = -\tfrac{1}{2}i\lambda^{(0)}_n(R^2_{(-1)}/R^2)\eta\phi^{(0)}_{n\eta} + \psi_n, \tag{4.12}$$

$$\psi_n = \sum_{m=0}^{\infty} \gamma_m(x)P_m(\eta), \tag{4.13}$$

where

$$\gamma_m = A_m \exp(-lx/\omega^{(0)}_m) + B_m \exp(-lx/\omega^{(0)}_n), \quad m \neq n, \quad m \geqslant 1, \tag{4.14a}$$

$$\gamma_n = (xD_n + x^2E_n)\exp(-lx/\omega^{(0)}_n), \tag{4.14b}$$

$$\gamma_0 = A_0 + B_0 \exp(-lx/\omega^{(0)}_n), \tag{4.14c}$$

$$A_0 = (\omega^{(0)}_n/l)[\varepsilon J_{n0} + \tfrac{1}{2}i\lambda^{(0)}_n(l/\omega^{(0)}_n)P_{n(-1)}], \tag{4.14d}$$

$$\begin{aligned}B_0 &= -(\omega^{(0)}_n/l)^2[-\tfrac{1}{2}i\lambda^{(0)}_n R^2_{(-1)}I_{n0} \\ &\quad + 2\varepsilon(l/\omega^{(0)}_n)J_{n0}],\end{aligned} \tag{4.14e}$$

$$\begin{aligned}A_m &= [(l/\omega^{(0)}_n) - (l/\omega^{(0)}_m)]^{-1} \\ &\quad \times [\varepsilon J_{nm} + \tfrac{1}{2}i\lambda^{(0)}_n(l/\omega^{(0)}_n)P_{n(-1)}P_{m(-1)}],\end{aligned} \tag{4.15a}$$

$$B_m = -[(l/\omega_n^{(0)})^2 - (l/\omega_m^{(0)})^2]^{-1}$$
$$\times [-\tfrac{1}{2}i\lambda_n^{(0)} R^2_{(-1)} I_{nm} + 2\varepsilon(l/\omega_n^{(0)}) J_{nm}], \quad (4.15b)$$

$$D_n = -\tfrac{1}{4}i\lambda_n^{(0)} R^2_{(-1)}(\omega_n^{(0)}/l)\, I_{nn} + \varepsilon[\tfrac{1}{2} + J_{nn}], \quad (4.15c)$$

$$E_n = \tfrac{1}{2}\varepsilon(l/\omega_n^{(0)}), \quad (4.15d)$$

$$J_{nm} = \int_{-1}^{0} \eta P_{n\eta} P_m \, d\eta. \quad (4.15e)$$

As in Section 3, the topographic correction to ω is $O(\varepsilon)$ and real, representing an increase in the phase speed, while the frictional correction to ω is $O(\lambda_n^{(0)})$ and imaginary, representing a spin down with time. There is an $O(\varepsilon)$ correction to the structure of ϕ and an $O(\lambda_n^{(0)})$ correction to the phase of ϕ. The topographic correction to the phase speed is due to the depth variation from a flat bottom weighted with the Rossby radius scale, i.e.,

$$(\omega_n^{(1)}/l)_{top} = \int_0^{\infty} \exp(-lx/\omega_n^{(0)})\, [1 - H(x)]\, dx. \quad (4.16)$$

With (4.1), $\omega_n^{(1)}$ calculated with (4.16) is equal to the first term in (4.11). The weak slope topography increases the effective depth (see Fig. 7) relative to a flat bottom at $Z = -1$, thus increasing the phase speed relative to the flat bottom case. A similar result was obtained by Allen (1975, eq. (3.15c)) with a two-layer model.

The $m = 0$ term in (4.13) represents a barotropic flow induced by both friction and topography. For $x \to \infty$, the baroclinic terms are exponentially small and $\phi_n^{(0)} \sim A_0$ which, with (3.5) and (2.3a, b), implies that far offshore, a barotropic onshore flow remains. The barotropic flow matches to an outer shelf solution that represents a forced topographic Rossby wave. This point has been discussed by Allen (1975) and Allen and Romea (1980) and will not be addressed further here.

Where $R = R_0$, simple analytical solutions for ϕ are again obtained. In particular, the correction to the O(1) frequency is

$$\omega_n^{(1)} = \tfrac{1}{2}\varepsilon R(n\pi)^{-1} - \tfrac{1}{4}iE_v^{1/2}. \quad (4.17)$$

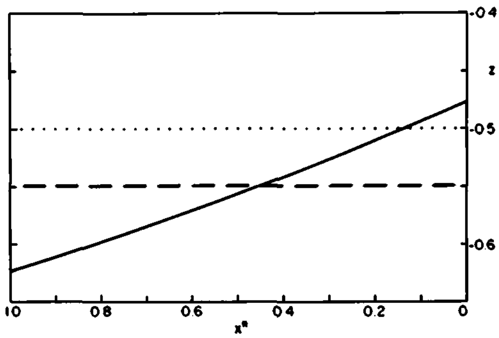

Fig. 8. Zero crossing for the $n = 1$ internal Kelvin wave for v in the x^*–z plane, with $\lambda = 0$, $\varepsilon = 0.1$, and $R = R_0$ (solid line). Dotted line: predicted zero crossing for corresponding flat bottom mode with bottom at $z = -1$. Dashed line: predicted zero crossing for corresponding flat bottom mode with bottom at $z = -1.05$. Weak slope model.

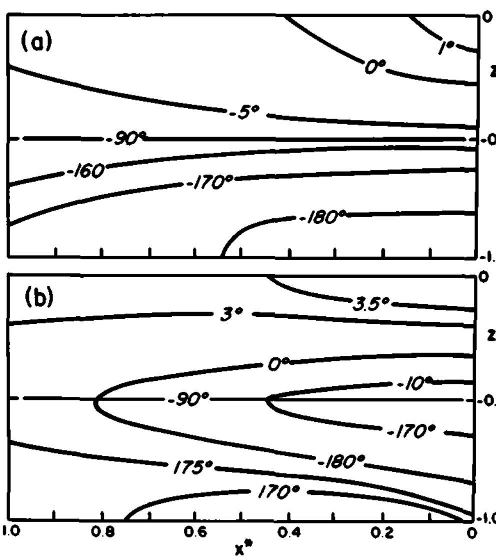

Fig. 9. Frictionally-induced phase shift θ (in degrees) in (a) p and (b) v for the first mode internal Kelvin wave in the x^*–z plane for $\lambda_1^{(0)} = 0.1$, $\varepsilon = 0$, and $R = R_0$. $\theta_1 > \theta_2$ implies 1 lags 2. Weak slope model.

Fig. 8 shows the zero crossing for the first mode of v in the x^*–z plane, where $x^* = \pi x/R$, $\lambda=0$, $\varepsilon = 0.1$, and $R = R_0$. Except for $x^* < 0.15$, the zero crossing is deeper than the zero crossing (at $Z = -0.5$) expected for an internal Kelvin wave with $n = 1$ and with a flat bottom at $z = -1$. Near $x^* = 0.5$, the zero crossing is near the predicted zero crossing for a flat bottom at a depth of $z = -1.05$, which is the averaged Rossby radius scale weighted depth. This result again illustrates the increased effective depth due to the sloping bottom.

Fig. 9a, b, show the frictionally induced phase shifts in p and v for the $n = 1$ mode internal Kelvin wave in the x^*–z plane for $\lambda_n^{(0)} = 0.1$ and $\varepsilon = 0$. Phase shifts for v and p are clearly different; however, vertical phase lags imply that both deeper

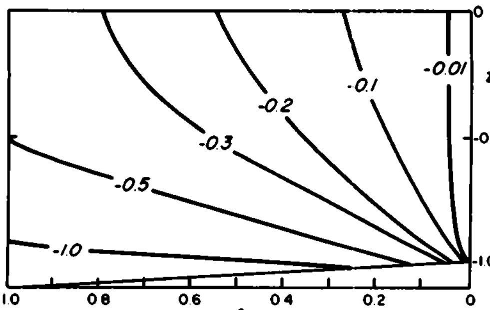

Fig. 10. Topographically-induced onshore flow u_T/ε in the x^*–z plane with $\lambda = 0$, $\varepsilon = 0.1$, and $R = R_0$, for the first mode internal Kelvin wave. Weak slope model.

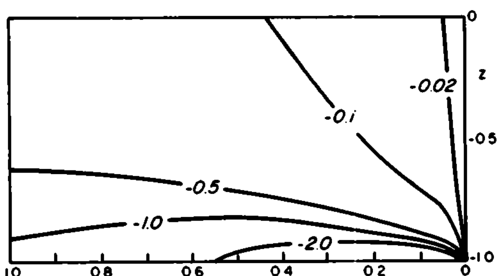

Fig. 11. Frictionally-induced onshore flow $u_F/\lambda_n^{(0)}$ in the x^*–z plane with $\varepsilon = 0$ and $R = R_0$, for the first mode internal Kelvin wave. Weak slope model.

v and p lead those above. In the upper half, p offshore leads p at the coast, while the effect is reversed for the lower layer. For v, offshore motions lead those inshore for $-0.1 > z > -0.5$, while inshore motions lead for $-1.0 < z < -0.5$ and $-0.1 < z < 0$.

Fig. 10 and 11 show the topographically-induced scaled onshore velocity u_T/ε (with $\lambda_1^{(0)} = 0$ and $\varepsilon = 0.1$) and the frictionally-induced scaled onshore velocity $u_F/\lambda_1^{(0)}$ (with $\varepsilon = 0$) for the $n = 1$ mode in the x^*–z plane with $R = R_0$. In each figure, $u \to 0$ as $x \to 0$, ($z \neq -1$) satisfying the boundary condition at $x = 0$. The flow u_F decreases offshore and upward, with a maximum at $x = 0$, $z = -1$, representing the mass flux out of the bottom Ekman layer required to satisfy (4.4). The flow u_T is largest directly over the slope and decreases upward and toward the coast.

5. Discussion

We have examined the effects of bottom Ekman layer friction and slope topography on free internal Kelvin waves, using both steep and weak slope models. Frictional effects are assumed weak and specific slope topographies are chosen so that perturbation methods may be used to obtain solutions. The steep slope model represents a low latitude case where the Rossby radius scale is assumed large compared to the slope width. The slope topography is a small perturbation along the side wall and the remainder of the bottom is flat. The bottom Ekman layer is continuous along the flat bottom interior and along the slope and intersects the surface at the coast. As a result, the frictional effect depends on the geometry of the slope. The weak slope model corresponds to the case where the Rossby radius scale is assumed to be much less than the slope width. The topography is assumed to be a small perturbation on a flat lower boundary, and a bottom Ekman layer intersects a vertical wall at $z = -H$, $x = 0$. For this case, we may examine frictional effects with a flat bottom or topographic effects in the absence of bottom friction.

The presence of bottom friction affects internal Kelvin waves in several ways. Free waves are damped with a dimensional time scale $T_f' = (\mu E_v^{1/2} f)^{-1}$ where $\mu = |\omega_n^{(1)}(\text{frictional})|/E_v^{1/2}$ is related to the frictional correction to the wave frequency. Phase shifts in x and z are induced as well as an onshore flow. There are substantial differences between the steep and weak slope models. We have obtained results with general stratification, and in order to elucidate these differences, we examine a particular more realistic stratification, but one which allows analytical solutions, i.e., an exponential N^2 profile (see (A1) in the Appendix). Details of the solution for the exponential stratification are presented in the Appendix.

Table 2 shows estimates of the dimensional spin down time scale T_f' for the first mode internal Kelvin wave for various s, where s is a measure of the exponential decay of N^2 with depth (A1). We choose $E_v^{1/2} = 0.02$ (Ekman depth = 40 m for H = 2 km) and $f = 1.3 \times 10^{-5}\ s^{-1}$ (5° latitude). In the Appendix, we show that $s = 3$ yields a reasonable approximation to the modal structure for the Peru case. For the weak slope, where friction acts

Table 2. *Ratio of bottom alongshore velocity $v_{(-1)}$ to surface alongshore velocity $v_{(0)}$ for the $n = 1$ internal Kelvin wave for various s, where the stratification is given by $R(z) = R_0 \exp(sz)$; also shown are $\mu = |\omega_1^{(1)}$ (frictional)$|/E_v^{1/2}$ for the weak and steep slope models; the dimensional spin down time is listed and is given by $T_f' = (E_v^{1/2} f\mu)^{-1}$, with $E_v^{1/2} = 0.02$ and $f = 1.3 \times 10^{-5}$ s^{-1} (5° latitude)*

		Weak slope			Steep slope		
s	$\lvert v_{(-1)}/v_{(0)}\rvert$	μ	$\mu/\lvert v_{(-1)}/v_{(0)}\rvert$	T_f' (days)	μ	$\mu\lvert v_{(-1)}/v_{(0)}\rvert$	T_f' (days)
0	1	0.5	0.5	89	0.5	0.5	89
0.5	0.79	0.39	0.49	114	0.64	0.50	70
1	0.61	0.30	0.49	148	0.80	0.49	56
2	0.40	0.19	0.48	234	1.2	0.48	37
3	0.28	0.13	0.46	342	1.6	0.45	28
5	0.17	0.08	0.44	594	2.6	0.44	17

through the Ekman compatibility condition at $z = -1$, which involves the bottom velocity, we expect that a more realistic N^2 profile will yield a smaller bottom velocity and hence the effect of friction will be reduced. Table 2 shows that the correction to the frequency due to friction decreases and the spin down time increases for increasing s, which supports the above argument. In addition, Table 2 shows that $\mu|v_{(-1)}/v_{(0)}|$ for the weak slope case is nearly constant and indicates that the spin down time is almost but not exactly proportional to the bottom velocity.

For the steep slope case, the effects of a more realistic N^2 profile are reversed, i.e., Table 2 shows that μ increases and T_f' decreases for increasing s. This is due to the fact that the mode interacts with the Ekman layer over the slope as well as on the bottom. It is for this reason that the neglect of bottom stress when considering baroclinic modes in coastal regions, while perhaps justifiable at high lattitudes, may not be reasonable for low latitudes.

The expansion procedure used for both the weak and steep slope problems becomes invalid when the wave period is the same order as the spin down time. Table 2 shows that with $E_v^{1/2} = 0.02$, this restriction is satisfied for $T \ll 28$ days.

The estimates for decay time are relatively long compared to estimates given by Brink and Allen (1978) (see also, Brink and Allen, 1983) for barotropic continental shelf waves at mid-latitudes, reflecting the dependence of spin down time on latitude and the inhibition of bottom friction effects by stratification. These long decay times may explain why free coastally trapped waves with $T = 5$–10 days are observed to propagate along the Peru coast between 2° S and 17° S latitude with little evidence of frictional decay (Smith, 1978; Romea and Smith, 1980).

Frictionally-induced phase shifts are proportional to $\lambda = E_v^{1/2}/\omega$ and are stronger for higher latitudes or lower frequency. Plots of the x–z phase dependence of p and v for the $n = 1$ mode internal Kelvin wave (Figs. 2a, b for the steep slope case and Figs. 9a, b for the weak slope case) indicate substantial qualitative differences between the two cases. Phase shifts in v for the steep slope case are largest near the surface, with a phase lag in x in 30° over the Rossby radius scale with motions at the coast leading. Surface motions lead those below, and the vertical phase lags are greatest near the surface and the coast. In contrast, phase shifts predicted for the weak slope case are much smaller and motions at the bottom lead those above.

The onshore flow due to friction u_F also depends on the model used. For the steep slope (Fig. 6), u_F is largest near $x = 0$, $z = 0$ due to the mass flux out of the Ekman layer at the point, while for the weak slope (Fig. 10) u_F is strongest near $x = 0$, $z = -1$.

Slope topography affects free internal Kelvin waves directly in several ways: there is a change in wave frequency and alongshore phase speed, the modal structure is altered, and an onshore flow is induced.

Changes in modal structure and phase speed due to topography for the weak slope case agree with arguments by Hogg (1980) that observations of baroclinic wave dynamics on a sloping bottom can be rationalized with internal modes on a flat bottom by defining an effective bottom depth as an average over the offshore decay scale. The expression

(4.16), which is the modification to the wave speed due to a weak slope, is analagous to the result obtained by Miles (1972) for barotropic Kelvin waves with the assumption that the shelf width is small compared to the external Rossby radius scale.

For the steep slope case, corrections to the free wave speed are dependent on details of the slope geometry. A slope that is concave downward (Fig. 4) acts to increase the speed while a slope that is concave upward decreases the speed. A linear slope induces a distortion to the x–z modal structure but does not affect the wave speed to first order. Most continental slopes are concave downward; therefore at low latitudes, we may expect to see wave speeds that are augmented relative to the predicted flat bottom wave speed. These results are different from Miles' result for barotropic Kelvin waves where the addition of a narrow slope always slows the wave speed relative to the speed with a vertical wall.

Brink (1982a) calculates free wave phase speeds for realistic stratification and topography using a numerical model and finds that, between 5° and 15° latitude, the wave speed is lower than the wave speed predicted with a vertical wall at the coast. This is in agreement with predictions from the weak slope model. Brink does not extend his analysis to lower latitudes; however there is a hint (see Brink, 1982a, Fig. 2) that the free wave phase speed begins to increase for latitudes less than 5°. This may reflect the increase in phase speed predicted with the steep slope model for $L_s/\delta_R \ll 1$ when the slope is concave downward.

The topographically-induced onshore flow u_T for the weak slope is strongest directly over the slope and increases offshore, matching to an outer slope solution consisting of a topographic Rossby wave. For the steep slope, u_T is strongest over the slope near the zero crossing of v, reflecting the interaction of the O(1) w, which has a maximum near $z = -\frac{1}{2}$, with the slope.

Brink's (1982b, Fig. 3) numerical calculation of free coastal trapped waves near 15° S latitude with bottom friction shows p at the bottom leading p above and p at the coast leading p offshore. These results agree with predictions from the weak slope model. An empirical orthogonal function (EOF) for the 0.1–0.2 cpd frequency band using alongshore velocity from the Lobivia and Lagarta moorings near 15° S over the slope off the Peru coast in 560 m of water (Romea and Smith, 1983, Fig. 15a) shows v at 215 m leaving v at 58 m by 19°. On the shelf near 15° S, at the Mila mooring in 120 m of water, an EOF for the same frequency band as above shows v at 115 m leading v at 19 m by 30°. Both these observations and the numerical calculation suggest that, at 15° S, where $L_s/\delta_R \sim O(1)$, the predictions of the weak slope modes are more appropriate.

An EOF for the 0.1–0.2 cpd frequency band using alongshore velocity at 5° S off the Peru coast from the C2 mooring over the slope in 1360 m of water (Romea and Smith, 1983, Fig. 15b) shows a phase shift from near the surface (86 m) to below the zero crossing for the EOF (860 m) of 190°, with the surface leading. This EOF and the EOF calculated for Lobivia and Lagarta are shown in Romea and Smith (1983) to represent first mode internal Kelvin waves. These observations at low latitude where $L_s/\delta_R \ll 1$ are in qualitative agreement with predictions from the steep slope model (Fig. 2).

6. Acknowledgements

This research was supported by the Oceanography Section of the National Science Foundation for R.D.R. under Grants OCE-7803382 and OCE-8024116 and for J.S.A. under Grants OCE-7826820 and OCE-8017929.

7. Appendix: exponential N^2 profile

We have obtained results for both steep and weak slope topographies with general stratification. We now examine a particular more realistic stratification, but one which still allows analytical solutions, i.e., an exponential N^2 profile given by

$$R(z) = R_0 \exp(sz), \tag{A1}$$

where R_0 = constant. Profiles of $R(z)$ are plotted for various s in Fig. 12.

The x–z structure of the O(1) solution is given by (3.14), where $P_n(z)$, the vertical modal structure, is obtained by solving (3.15), (3.16) and (3.17) with the appropriate R. with (A1), the eigenvalue problem yields

$$\phi_n^{(0)} = \zeta^{1/2} \exp(-lx/\omega_n^{(0)}) [J_1(l\zeta^{1/2}/\omega_n^{(0)} s) + G_n Y_1(l\zeta^{1/2}/\omega_n^{(0)} s)], \tag{A2}$$

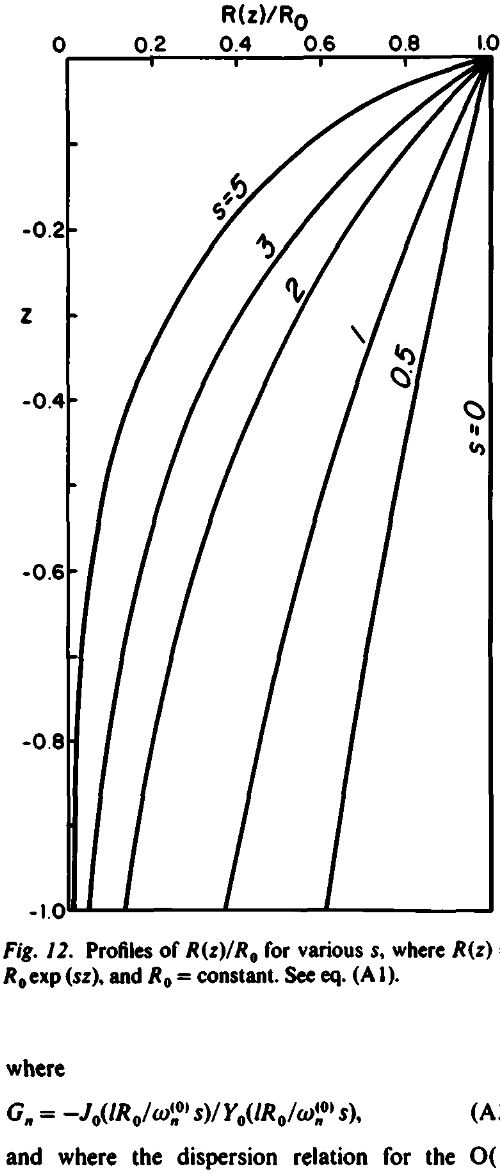

Fig. 12. Profiles of $R(z)/R_0$ for various s, where $R(z) = R_0 \exp(sz)$, and R_0 = constant. See eq. (A1).

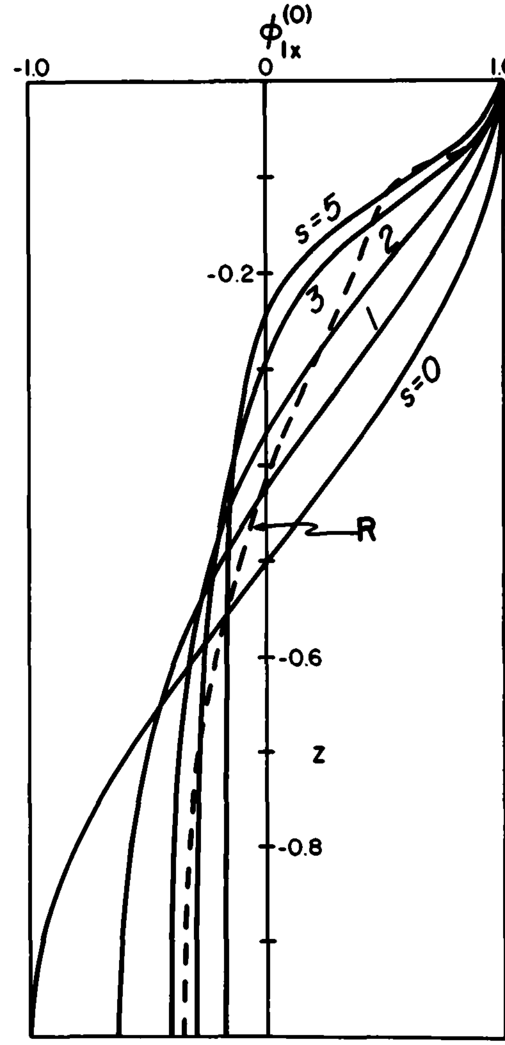

Fig. 13. Vertical structure for v for the first mode internal Kelvin wave for various s (see eq. (A1)). The modes are rescaled such that $v(x = 0, z = 0) - 1$. Also shown is the first dynamical mode (labelled R) calculated using the N^2 profile shown in Fig. 14.

where

$$G_n = -J_0(lR_0/\omega_n^{(0)} s)/Y_0(lR_0/\omega_n^{(0)} s), \tag{A3}$$

and where the dispersion relation for the O(1) eigenvalue $\omega_n^{(0)}$ is

$$J_0[lR_0 \exp(-s)/\omega_n^{(0)} s] + G_n Y_0[lR_0 \exp(-s)/\omega_n^{(0)} s] = 0. \tag{A4}$$

J_0, J_1, Y_0 and Y_1 are Bessel functions of the first and second kind of order 0 and 1 and

$$\zeta(z) = R^2(z) = R_0^2 \exp(2sz). \tag{A5}$$

The vertical structure of $\phi_{1x}^{(0)}$, which corresponds to alongshore velocity, is plotted in Fig. 13 for various s, where the modes are rescaled so that $P_{1(0)} = 1$. This is the O(1) modal solution, which is unaffected to first order by friction or topography and is the same for both the steep and weak slope problems. As s increases, the zero crossing of the mode becomes shallower and the bottom velocity decreases in accordance with the constraint of zero depth integrated mass flux in each mode, which follows from the integration over z of $P_n^{(0)}$ and the

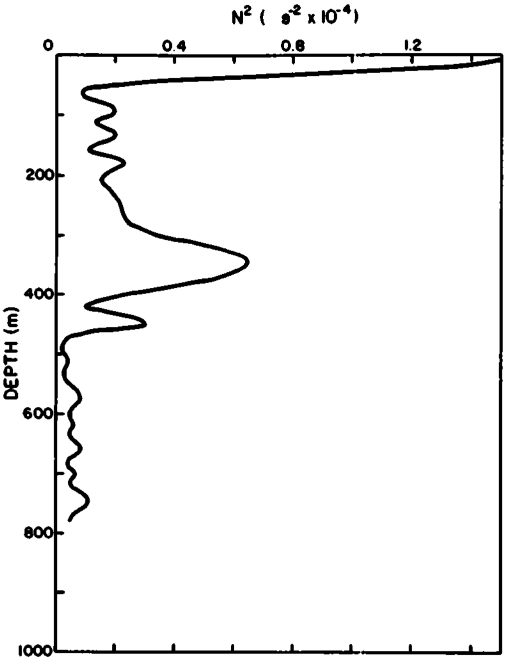

Fig. 14. N^2 profile, smoothed with a three-point moving average, calculated from CTD observations at 4°58.9′ S, 81°33.0′ W on May 22, 1977. The procedure used to obtain and process the CTD data is discussed by Huyer et al. (1978).

use of (3.13a). The ratio $|v(z = 0)/v(z = -1)|$ is shown in Table 2 as a function of s.

Fig. 14 shows a smoothed N^2 profile calculated from measurements taken near 5° S latitude over the slope. The vertical structure of v associated with the first dynamical mode (the dashed curve labelled R in Fig. 13), obtained numerically with the stratification shown in Fig. 14, indicates that the bottom velocity is a fraction of that predicted by the solution for constant stratification (the curve labelled $s = 0$ in Fig. 13). The mode shape was computed by integrating the governing equations by means of a fourth order Runge–Kutta technique, with a trial and error procedure for obtaining the proper eigenvalue so that the boundary conditions are satisfied (see Kundu et al., 1975, Section 5, for a discussion of the method). The profile was extrapolated to $N^2 = 0.1 \times 10^{-5}\ \mathrm{s}^{-2}$ at the bottom at 4 km depth by an exponential profile below 780 m depth (parameter studies indicate that the modal structure is relatively insensitive to the exact choice of exponential structure). Although the N^2 profile is different from the exponential profiles, the mode shape for s between 2 and 3, particularly near $z = -1$, is a reasonable approximation to the vertical structure calculated with the N^2 profile shown in Fig. 14; we therefore expect estimates of frictional effects to be more realistic with s between 2 and 3 than with $s = 0$.

Corrections to ω may be obtained using (A2), (A3) and (A4) in (3.20) for the steep slope and (4.11) for the weak slope. The $O(\lambda_1^{(0)})$ frictional corrections to ω for both cases are shown in Table 2 for various s. Table 2 is discussed in Section 5.

REFERENCES

Allen, J. S. 1973. Upwelling and coastal jets in a continuously stratified ocean. *J. Phys. Oceanogr. 3*, 245–257.

Allen, J. S. 1975. Coastal trapped waves in a stratified ocean. *J. Phys. Oceanogr. 5*, 300–325.

Allen, J. S. and Romea, R. D. 1980. On coastal trapped waves at low latitudes. *J. Fluid Mech. 98*, 555–585.

Allen, J. S. and Smith, R. L. 1981. On the dynamics of wind-driven currents. *Phil. Trans. R. Soc. Lond. A 302*, 617–634.

Brink, K. H. 1982a. A comparison of long coastal trapped wave theory with observations off Peru. *J. Phys. Oceanogr. 12*, 897–913.

Brink, K. H. 1982b. The effect of bottom friction on low frequency coastal trapped waves. *J. Phys. Oceanogr. 12*, 127–133.

Brink, K. H. and Allen, J. S. 1978. On the effect of bottom friction on barotropic motion over the continental shelf. *J. Phys. Oceanogr. 8*, 919–922.

Brink, K. H., Allen J. S. and Smith, R. L. 1978. A study of low frequency fluctuations near the Peru coast. *J. Phys. Oceanogr. 8*, 1025–1041.

Brink, K. H., Halpern, D. and Smith, R. L. 1980. Circulation in the Peruvian upwelling system near 150° S. *J. Geophys. Res. 85*, 4036–4048.

Brink, K. H. and Allen, J. S. 1983. Reply. *J. Phys. Oceanogr. 13*, 149–150.

Clarke, A. J. 1977. Observational and numerical evidence for wind-forced coastal trapped long waves. *J. Phys. Oceanogr. 7*, 231–247.

Hogg, N. G. 1980. Observations of internal Kelvin waves trapped round Bermuda, *J. Phys. Oceanogr. 10*, 1353–1376.

Huthnance, J. M. 1975. On trapped waves over a continental shelf. *J. Fluid Mech. 69*, 689–704.

Huthnance, J. M. 1978. On coastal trapped waves: analysis and numerical calculation by inverse iteration. *J. Phys. Oceanogr. 8*, 74–92.

Huyer, A., Gilbert, W. E., Schramm, R. and Barstow, D. 1978. CTD observations off the coast of Peru, R/V Mellville 4 March–22 May 1977, and R/V Columbus Iselin, 5 April–19 May 1977. Data report 71, Oregon State University, Reference 78–18, 409 pp.

Kundu, P. K., Allen, J. S. and Smith, R. L. 1975. Modal decomposition of the velocity field near the Oregon coast. *J. Phys. Oceanogr. 5*, 683–704.

Martinsen, E. A. and Weber, J. E. 1981. Frictional influence on internal Kelvin waves. *Tellus 33*, 402–410.

Miles, J. W. 1972. Kelvin waves on oceanic boundaries. *J. Fluid Mech. 55*, 113–127.

Pedlosky, J. 1974. On coastal jets and upwelling in bounded basins. *J. Phys. Oceanogr. 4*, 318.

Pedlosky, J. 1979. *Geophysical fluid dynamics*. Springer-Verlag, New York.

Romea, R. D. and Smith, R. L. 1983. Further evidence for coastal trapped waves along the Peru coast. *J. Phys. Oceanogr. 13*, 1341–1356.

Smith, R. L. 1978. Poleward propagating perturbations in sea level and currents along the Peru coast. *J. Geophys. Res. 83*, 6083–6092.